Ferroquadrupolar ordering in a magnetically ordered state in ErNiAl

Isao Ishii,[*] Yuki Kurata, Yuki Wada, Minoru Nohara ⓘ, and Takashi Suzuki[†]
Department of Quantum Matter, AdSE, Hiroshima University, Higashi-Hiroshima 739-8530, Japan

Koji Araki
Department of Applied Physics, National Defense Academy, Yokosuka, Kanagawa 239-8686, Japan

Alexander V. Andreev ⓘ
FZU Institute of Physics, Czech Academy of Sciences, Na Slovance 2, 182 21 Prague, Czech Republic

We conducted ultrasonic measurements to clarify whether a phase transition exists in ErNiAl, a hexagonal compound, below the antiferromagnetic transition temperature, $T_N \sim 6$ K. We discovered a significant elastic softening of the transverse modulus, C_{66}, accompanied by a significant ultrasonic attenuation toward $T_Q = 3.4$ K, which is the temperature of a sharp downward peak in other moduli, indicating a phase transition at T_Q. The crystal field analysis reveals that the softening of C_{66} below 80 K is due to an interlevel O_{xy}-type quadrupole interaction with a positive quadrupole-quadrupole coupling constant between the ground and excited Kramers doublets. A spontaneous expectation value of O_{xy} emerges at T_Q in our crystal field model with the mean-field approximation. No quadrupolar ordering occurs in a magnetically ordered state because the degeneracy of quadrupoles is lifted by an internal magnetic field of magnetic ordering. However, our experimental and calculated results suggest that the driving force of the phase transition at T_Q is O_{xy}-type ferroquadrupolar ordering, implying a quadrupolar ordering in a magnetically ordered state at zero magnetic field.

I. INTRODUCTION

Rare-earth compounds with localized f electrons show attractive physical properties due to the orbital degrees of freedom, such as multipolar ordering and superconductivity [1–3]. The electric and magnetic multipole due to the orbital degrees of freedom are often significant in understanding their physical properties. Under a crystal electric field (CEF), an orbitally degenerate state of the $4f$-electronic state is expected in compounds with higher symmetry, such as a cubic structure. By contrast, compounds with lower symmetry, such as an orthorhombic structure, have attracted less attention for multipole interactions due to a singlet or Kramers doublet ground state.

However, an interlevel multipole interaction between the ground state and excited states exists even in low-symmetry compounds. The magnitude of the interaction depends on an energy splitting of the CEF and a coupling constant of the multipole. Recently, we reported the existence of a quadrupole interaction in DyNi$_3$Ga$_9$, R_3Ru$_4$Al$_{12}$, and DyNiAl, where R is the heavy rare earth [4–10]. These compounds have trigonal, hexagonal, and orthorhombic CEF, respectively. The energy splitting between the ground state and excited states is relatively small in these compounds. Notably, DyNi$_3$Ga$_9$ shows a ferroquadrupolar ordering and a magnetic-field-induced

quadrupolar ordering was discovered in Dy$_3$Ru$_4$Al$_{12}$ and DyNiAl [4,7,10].

In this study, we paid attention to the Er-based compound, ErNiAl, which has a hexagonal ZrNiAl-type structure (space group $P\bar{6}2m$) consisting of Er-Ni and Al-Ni layers stacked alternately along [001] [11–16]. The Er ions form a kagomelike triangular lattice in the (001) plane, and their site symmetry is orthorhombic, C_{2v} [17]. A clear peak at $T_N \sim 6$ K due to an antiferromagnetic ordering was observed in the specific heat measurement [12–14]. The neutron diffraction experiment at 1.8 K revealed a triangle magnetic structure in which all magnetic moments are in the (001) plane [11]. In addition, a possibility of an additional phase transition below T_N was suggested in a polycrystalline sample; however, it is unclear [11].

The magnetic susceptibility, χ, obeys the Curie-Weiss law above 25 K for a magnetic field applied along [001] and perpendicular to [001] [14]. The effective magnetic moments for both axes were determined to be $9.51\mu_B$. This value is almost the same as the theoretical value of the free Er^{3+}, $9.59\mu_B$. ErNiAl has the CEF effect, and the Er^{3+} 16-fold multiplet (total angular momentum $J = 15/2$) splits into eight Kramers doublets under the orthorhombic CEF. The CEF-level scheme at the low-energy region was presented as the first excited doublet at 9 K, the second excited doublet at 31 K, and the third excited doublet at 80 K, based on the inelastic-neutron scattering experiment [12,14–16]. The multipole interactions are also expected in ErNiAl because the first excited doublet exists near the ground doublet.
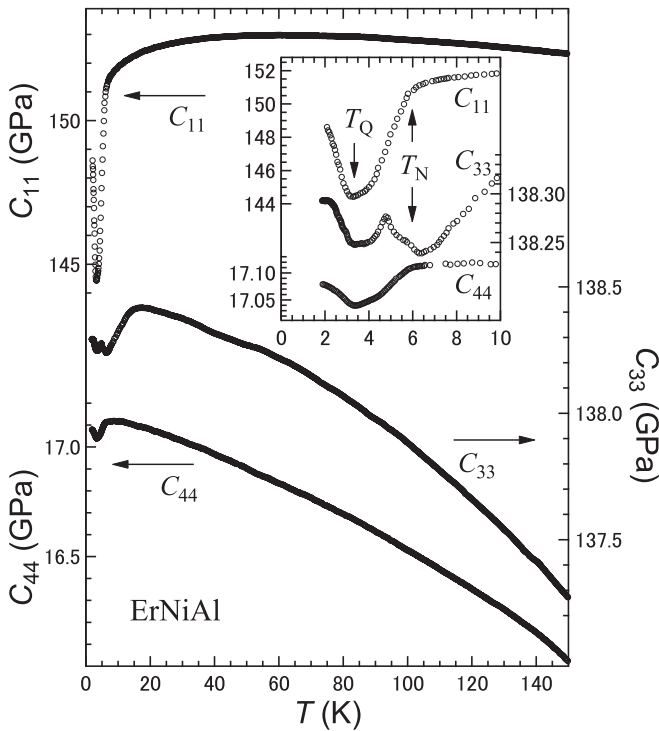
[*]ish@hiroshima-u.ac.jp
[†]tsuzuki@hiroshima-u.ac.jp

FIG. 1. Temperature dependence of the longitudinal elastic moduli C_{11} (left upper axis) and C_{33} (right axis) as well as the transverse modulus C_{44} (left lower axis) in ErNiAl. The inset displays the same data on an expanded temperature scale below 10 K. The vertical arrows indicate the phase transitions at T_N and T_Q.

Ultrasonic measurements are a great tool for investigating quadrupole interactions because a strain induced by ultrasound bilinearly couples to a corresponding quadrupole moment [18–27]. We measured the elastic moduli on single-crystalline samples using the ultrasonic technique to clarify a possibility of a phase transition below T_N and quadrupole interactions in ErNiAl.

II. EXPERIMENTAL DETAILS

Single crystals of ErNiAl were grown using a modified Czochralski method [28]. X-ray powder-diffraction analysis showed that the sample is in a single phase. The lattice parameters are the same as in Ref. [14], $a = 6.972$ Å and $c = 3.799$ Å. The temperature dependence of the elastic moduli C_{11}, C_{33}, C_{44}, and C_{66} was measured between 1.8 and 150 K using a phase comparison-type pulse-echo method [29]. For the longitudinal moduli, C_{11} and C_{33}, the propagation, $\boldsymbol{k}$, and displacement, $\boldsymbol{u}$, directions of the ultrasound are $\boldsymbol{k} \parallel \boldsymbol{u} \parallel [100]$ and $\boldsymbol{k} \parallel \boldsymbol{u} \parallel [001]$, respectively. The transverse elastic moduli, C_{44} and C_{66}, were measured by ($\boldsymbol{k} \parallel [001]$, $\boldsymbol{u} \parallel [100]$) and ($\boldsymbol{k} \parallel [100]$, $\boldsymbol{u} \parallel [120]$) configurations, respectively. The elastic modulus, C, was calculated from the equation $C = \rho v^2$, with the mass density, $\rho = 7.879$ g/cm^3. The absolute value of the sound velocity, v, was determined at 150 K for each mode using the sample length and a time interval between pulse echoes. The temperature dependence of ultrasonic attenuation for C_{66} was measured below 15 K using an orthogonal phase-detection method [30]. We used LiNbO$_3$ transducers
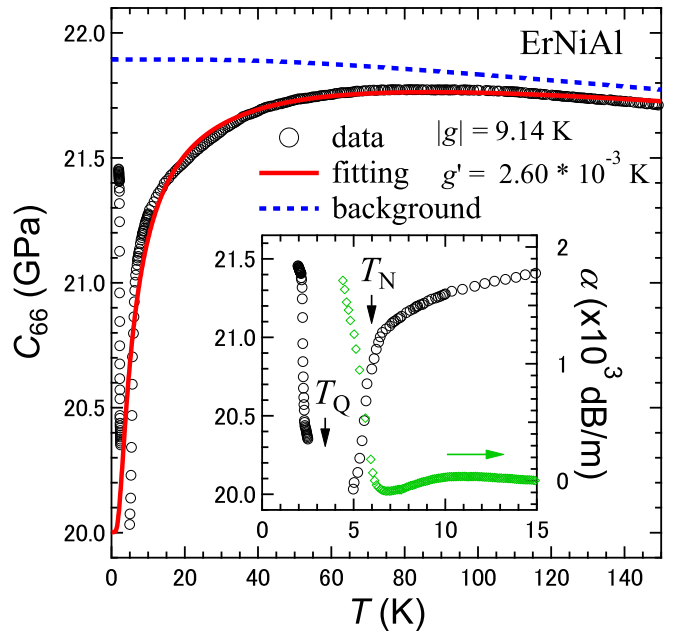

FIG. 2. Temperature dependence of the transverse elastic modulus C_{66} in ErNiAl. The inset represents C_{66} (left axis) and its ultrasonic attenuation α (right axis) near T_N and T_Q. The vertical arrows indicate phase transitions. The red solid and blue dashed lines show the fit result and the background stiffness, respectively.

with a fundamental resonance frequency of about 30 MHz. A commercial physical property measurement system was used for the specific heat measurement from 2 to 30 K. Magnetic susceptibility and magnetization were measured from 2 to 300 K and up to 5 T, respectively, using a commercial magnetic property measurement system (MPMS) with a superconducting magnet.

III. RESULTS AND DISCUSSION

A. Elastic modulus, specific heat, and magnetic susceptibility

Figure 1 shows the temperature dependence of the longitudinal elastic moduli, C_{11} and C_{33}, and the transverse modulus, C_{44}, in ErNiAl. These moduli increase monotonically as the temperature decreases to 80 K. An elastic softening of C_{11} is detected below 80 K. The inset of Fig. 1 shows that as the temperature further decreases, C_{11} changes the slope at T_N and then rapidly decreases. A downward peak is observed at $T_Q = 3.4$ K. By contrast, C_{33} and C_{44} continue to harden below 80 K. C_{33} softens below 15 K and exhibits downward peaks at both T_N and T_Q. The transverse modulus, C_{44}, starts to decrease around T_N and displays a downward peak at T_Q. These clear peaks at T_Q suggest an as-yet-unidentified phase transition.

Figure 2 shows the temperature dependence of the transverse elastic modulus, C_{66}, in ErNiAl. C_{66} increases monotonically as the temperature decreases below 150 K. C_{66}, like C_{11}, shows an elastic softening below 80 K and a change in the slope at T_N. The softening of C_{66} below 80 K is a characteristic behavior due to a quadrupole interaction in the CEF. We discovered a significant elastic softening toward T_Q with a more than 5% reduction in the stiffness below
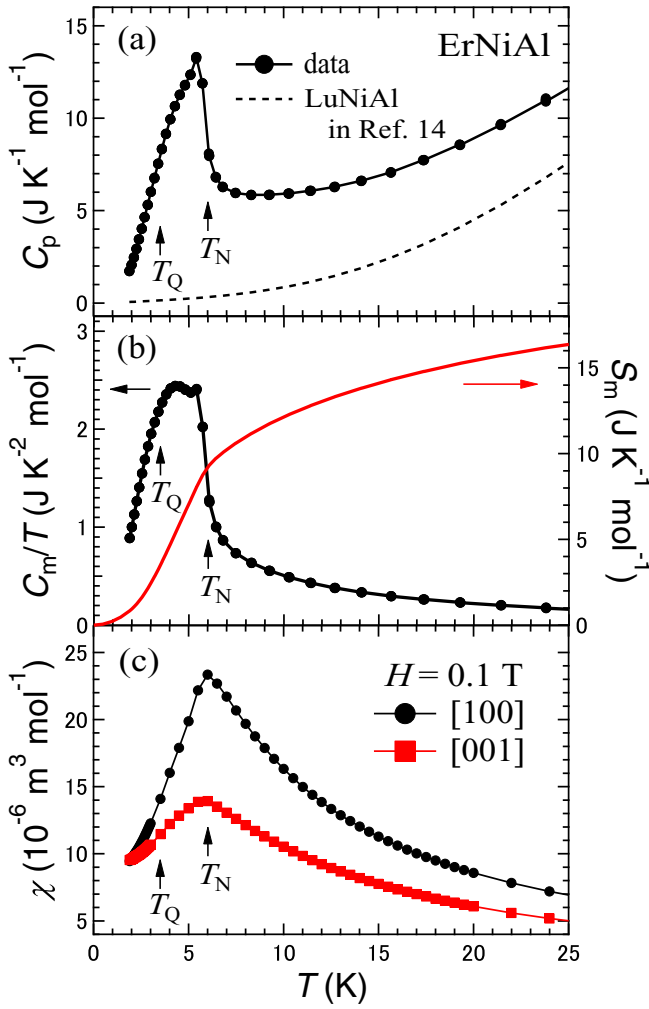
FIG. 3. Temperature dependence of (a) the specific heat at zero field, (b) magnetic specific heat divided by the temperature C_m/T (left axis) and magnetic entropy S_m (right axis), and (c) magnetic susceptibility measured at 0.1 T. The specific heat of the reference compound LuNiAl was taken from Ref. [14]. The obtained data are consistent with the reported data [12–14,16].

T_N as the temperature further decreases. The ultrasonic pulse echoes fade away toward T_Q due to significant enhancement of ultrasonic attenuation, as shown in the inset of Fig. 2; thus, C_{66} cannot be measured around T_Q.

We measured the specific heat, C_p, at zero magnetic field and the magnetic susceptibility, χ, for a magnetic field of 0.1 T applied along [100] and [001] to investigate the phase transition at T_Q in detail (Fig. 3). In addition to a sharp peak at T_N, C_p shows a broad kink around T_Q, suggesting a phase transition [Fig. 3(a)]. We estimated the magnetic specific heat, C_m, contributed by $4f$ electrons by subtracting C_p of the reference compound LuNiAl from C_p of ErNiAl [Fig. 3(b)]. The magnetic entropy released is about $0.6 \times R_g \ln 2$ at T_Q and exceeds $R_g \ln 2$ at T_N, where R_g is the gas constant.

Both χ for the field applied along [100] and [001] follow the Curie-Weiss law at high temperatures [Fig. 3(c)]. These results are consistent with the previously reported data [12–14,16]. In contrast to a visible cusp-type anomaly at T_N, there is no clear anomaly at T_Q in both χ, implying that the

driving force of the phase transition at T_Q is not a simple magnetic interaction. Notably, the C_{66} mode corresponding to the ε_{xy} strain shows a significant softening toward T_Q as well as significant ultrasonic attenuation. Consequently, we discovered a phase transition at T_Q that has no magnetic origin.

B. Crystal-electric-field effects

Determining the $4f$-electronic state is critical in the localized f-electron system for investigating the origin of the phase transition at T_Q. We performed a CEF analysis for C_{66}, $1/\chi$, and magnetization, M, curves in the nonordered state to determine the $4f$-electronic state and investigate quadrupole interactions in ErNiAl. Here, we adopted the orthorhombic CEF because the site symmetry of the Er^{3+} is orthorhombic [17]. We considered the following effective Hamiltonian H_{eff}:

$$H_{eff} = H_{CEF} + H_Q + H_{Zeeman},$$
$$H_{CEF} = B_2^0 O_2^0 + B_2^2 O_2^2 + B_4^0 O_4^0 + B_4^2 O_4^2 + B_4^4 O_4^4$$
$$+ B_6^0 O_6^0 + B_6^2 O_6^2 + B_6^4 O_6^4 + B_6^6 O_6^6,$$
$$H_Q = -g_{xy} O_{xy} \varepsilon_{xy} - g'_{xy} \langle O_{xy} \rangle O_{xy},$$
$$H_{Zeeman} = -g_J \mu_B J H,$$

where H_{CEF}, H_Q, and H_{Zeeman} are Hamiltonians of the CEF, the quadrupole interaction, and the Zeeman interaction, respectively. g_{xy}, g'_{xy}, O_{xy}, B_m^n ($n = 0$, 2, 4, 6, and $m = 2$, 4, and 6), and O_m^n are the strain-quadrupole coupling constant, quadrupole-quadrupole coupling constant, quadrupole operator, CEF parameter, and Stevens equivalent operator, respectively [31]. $\langle O_{xy} \rangle$ represents the thermal average of O_{xy}.

The quadrupole interaction term, H_Q, was used only for C_{66}. The modulus C_{66} is the linear response to the ε_{xy} strain, which couples to the electric quadrupole $O_{xy} = (J_x J_y + J_y J_x)/2$. The temperature dependence of C_{66} was calculated using the following equation:

$$C_{66}(T) = C_0 \left[\frac{1 - (N_0 g_{xy}^2 / C_0 + g'_{xy}) \chi_s(T)}{1 - g'_{xy} \chi_s(T)} \right], \quad (1)$$

where N_0 ($= 1.876 \times 10^{28}$ m^{-3}) is the number of Er^{3+} per unit volume and χ_s is the strain susceptibility [32,33]. We adopted the Varshni equation as the temperature dependence of the background stiffness, C_0 [34]:

$$C_0(T) = C_{0\,K} - \frac{s}{\exp(\theta_D/T) - 1}, \quad (2)$$

where $C_{0\,K}$ is the elastic modulus at 0 K, θ_D is the Debye temperature, and s is a fitting parameter [35].

We repeated the CEF fits using different initial CEF parameter values to reproduce C_{66} and $1/\chi$. Then, we changed all parameters in various combinations to reproduce M curves and the CEF-level scheme in the low-energy region reported [12,14–16]. The red solid curve in Fig. 2 is the best fit in the nonordered state. The softening of C_{66} above T_N is well reproduced with the fit parameters listed in Tables I and II. The ground doublet Γ_5, the first excited doublet Γ_5 at 8 K, the second excited doublet Γ_5 at 32 K, the third excited doublet Γ_5 at 81 K, and many others, are the obtained CEF-level scheme [Fig. 4(a)]. This CEF scheme up to the third excited state is consistent with the scheme reported by the inelastic-neutron

TABLE I. CEF parameters of ErNiAl in Kelvin.

B_2^0	B_2^2	B_4^0	B_4^2	B_4^4	B_6^0	B_6^2	B_6^4	B_6^6
-0.10	-1.40	-5.00×10^{-4}	-3.70×10^{-3}	2.80×10^{-2}	-5.50×10^{-5}	-2.15×10^{-4}	-1.00×10^{-5}	2.00×10^{-4}

scattering experiment [12,14–16]. Under the orthorhombic CEF, the $4f$-electronic state of the Er^{3+} ($J = 15/2$) splits into eight Kramers doublets with no quadrupole degeneracy. Because the only ground Kramers doublet does not produce elastic softening, our fit result reveals that the softening of C_{66} is due to an interlevel O_{xy}-type quadrupole interaction between the ground and excited doublets. The interaction of O_{xy} is of ferroquadrupolar type because the sign of g'_{xy} is positive (Table II).

The longitudinal modulus, C_{11}, softens below 80 K (Fig. 1). The moduli C_{66} and $(C_{11} - C_{12})/2$ are degenerate in the hexagonal symmetry. C_{11} corresponding to the ε_{xx} strain is affected by the elastic behavior of $(C_{11} - C_{12})/2$, which corresponds to the $\varepsilon_{xx} - \varepsilon_{yy}$ strain. The softening of C_{11} above T_N may be due to the quadrupole interaction corresponding to $(C_{11} - C_{12})/2$, as with DyNi$_3$Ga$_9$ and Tb$_3$Ru$_4$Al$_{12}$ [4,6]. On the other hand, there remains another possibility that a softening of the bulk modulus relating to the bulk $\varepsilon_B = \varepsilon_{xx} + \varepsilon_{yy} + \varepsilon_{zz}$ and $\varepsilon_{xx} + \varepsilon_{yy}$ strains causes the softening of C_{11}, such as in UCu$_2$Sn and La$_{2-x}$Sr$_x$CuO$_4$, respectively [18,36].

Figures 4(b) and 4(c) illustrate the fit results for $1/\chi$ in 0.1 T and M curves at 10 K, respectively. Here, $1/\chi$ and M were calculated using the aforementioned CEF model: $H_{CEF} + H_{Zeeman}$ [37,38]. The experimental data and theoretical calculations above T_N are consistent in both $1/\chi$ [Fig. 4(b)]. The calculated results at low fields accurately reflect the gradient of M curves at 10 K in the magnetic field applied along [100] and [001] [Fig. 4(c)]. Although the calculations deviate from the experimental data above 2.2 and 2.8 T along [100] and [001], respectively, the reason is currently unclear because no magnetic-field-induced phase transition was reported above T_N. These results clarify the $4f$-electronic state reproducing C_{66}, $1/\chi$, and M curves in the nonordered state.

C. Driving force of the phase transition at T_Q

Further, we discuss the origin of the phase transition at T_Q. Both χ in the field applied along [100] and [001] exhibit no anomaly at T_Q [Fig. 3(c)]. The transverse modulus, C_{66}, shows substantial softening toward T_Q, as well as significant ultrasonic attenuation (Fig. 2). These results indicate that the phase transition at T_Q arises from no magnetic origin and that the quadrupole O_{xy} plays a crucial role in the transition. To investigate an order parameter's expectation value,

we calculated C_m with the phase transition temperatures and spontaneous expectation values of J_x, J_y, J_z, and O_{xy} using the equation consisting of $H_{CEF} + H_{ex}$, where H_{ex} is the Hamiltonian of the spin and quadrupole exchange interactions in the mean-field approximation:

$$H_{ex} = -\sum_{j=A,B} \left\{ J_{exx}^{AB} \langle J_x \rangle^{(j)} J_x + J_{exy}^{AB} \langle J_y \rangle^{(j)} J_y \right.$$
$$\left. + J_{exz}^{AB} \langle J_z \rangle^{(j)} J_z + g_{ex}^{AB} \langle O_{xy} \rangle^{(j)} O_{xy} \right\},$$

where J_{ex}^{AB} and g_{ex}^{AB} are the coupling constant of intersublattice spin and quadrupole exchange interactions, respectively, and the symbols A and B denote two sublattices [39]. The subscripts x, y, and z correspond to [100], [120], and [001], respectively.

The calculated C_m is shown in the upper panel of Fig. 4(d). C_m with the transition temperatures of T_N and T_Q is well reproduced using $J_{exx}^{AB} = J_{exy}^{AB} = -0.294$ K, $J_{exz}^{AB} = 0$ K, and
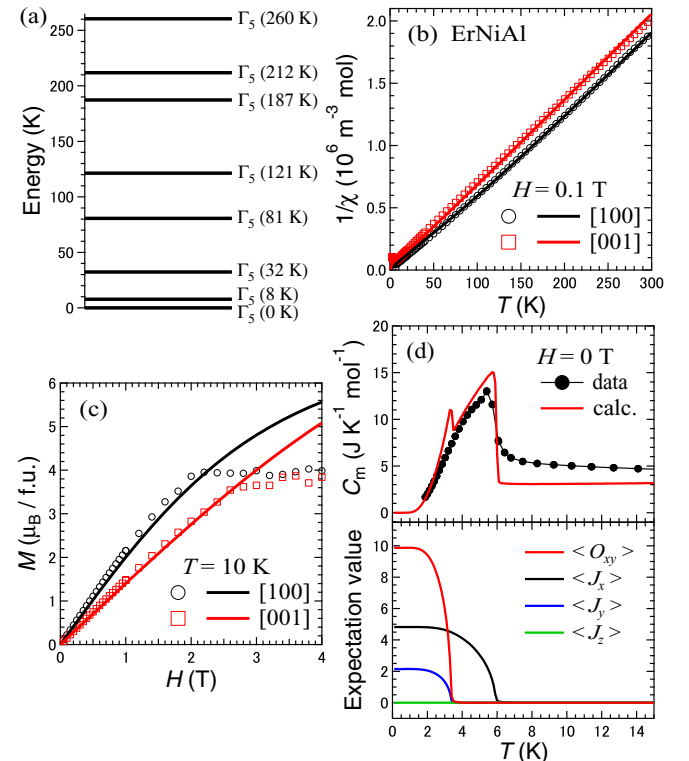

FIG. 4. (a) The $4f$-level scheme for ErNiAl obtained from the CEF parameters listed in Table I, where Γ_5 denotes the irreducible representation for the point symmetry C_{2v}. (b) Temperature dependence of the inverse magnetic susceptibility measured at 0.1 T. (c) Magnetization curves at 10 K. Solid lines represent the calculated results. (d) Temperature dependence of the calculated C_m (upper panel) and spontaneous expectation values of J_x, J_y, J_z, and O_{xy} (lower panel) at zero magnetic field.

TABLE II. Fitting parameters of C_{66}: $|g_{xy}|$ (K), g'_{xy} (K), $C_{0\,K}$ (GPa), θ_D (K), and s (GPa). We adopted the value of θ_D from the specific heat [14].

	$|g_{xy}|$	g'_{xy}	$C_{0\,K}$	θ_D	s
C_{66}	9.14	2.60×10^{-3}	21.9	150	0.21

$g_{ex}^{AB} = g'_{xy} = 2.60 \times 10^{-3}$ K. Here, negative values for J_x and J_y (zero for J_z) reflected the reported magnetic structure, which is the antiferromagnetic ordering in the (001) plane for spins [11]. We used the obtained g'_{xy} for the quadrupole O_{xy} (Table II). The lower panel of Fig. 4(d) shows the temperature dependence of expectation values of J_x, J_y, J_z, and O_{xy} at zero magnetic field. As the temperature decreases, $\langle J_x \rangle$ occurs at T_N, and then $\langle O_{xy} \rangle$ and $\langle J_y \rangle$ appear simultaneously at T_Q. The magnitude of $\langle O_{xy} \rangle$ is considerably larger than $\langle J_y \rangle$, implying that the driving force of the phase transition at T_Q is the quadrupole interaction of O_{xy}.

In almost all compounds, quadrupole interactions weaken below the magnetic transition temperature due to splitting of the CEF states by a local internal magnetic field of magnetic ordering, and substantial softening of the elastic modulus due to the quadrupole interaction disappears [6,7]. However, in ErNiAl, the elastic softening of C_{66} increases below T_N more than that of the calculated result in the nonordered state (Fig. 2). This result implies that the quadrupole interaction of O_{xy} remains even below T_N, being particularly strong between the CEF states separated by magnetic ordering.

We considered the reasons causing this situation. The magnetic ordering at T_N has a small splitting energy among the calculated ground doublet, and these states do not intersect with the first excited doublet. The wave functions of the CEF states are mixed by an energy of the internal field by the magnetic ordering linked to $\langle J_x \rangle$. Besides ErNiAl having a strong quadrupole O_{xy} interaction with a substantial softening of C_{66}, the ground two states have the O_{xy} interaction below T_N. The electronic population as the ground two states would sufficiently cause a phase transition.

As a result of these experimental data and calculations, we discovered O_{xy}-type ferroquadrupolar ordering at T_Q in a magnetically ordered state at zero magnetic field, making ErNiAl a unique compound because it exists in an electronic environment where quadrupolar ordering is impossible in principle. In addition, we also assessed the spontaneous expectation values of magnetic octupoles because a quadrupolar ordering appears in a magnetically ordered state [40]. Within our calculations, those of octupoles $\langle T_y^\alpha \rangle$ and $\langle T_y^\beta \rangle$ appear simultaneously with $\langle O_{xy} \rangle$ and $\langle J_y \rangle$ at T_Q. The octupoles may facilitate a cross correlation between ordered spins and spontaneous strains. In future studies, it may be necessary to consider the influence of magnetic octupoles.

IV. CONCLUSION

We investigated the elastic moduli in the ErNiAl antiferromagnet. The elastic softening due to the interlevel O_{xy}-type quadrupole interaction was detected below 80 K in the transverse modulus, C_{66}, and the softening increases below T_N. Because all moduli display an obvious downward peak at T_Q, we discovered a phase transition. The CEF parameters were determined to reproduce C_{66}, $1/\chi$, and M curves in the nonordered state. The calculated C_m using the CEF model with the mean-field approximation explains the phase transitions at T_N and T_Q. The expectation value of the quadrupole O_{xy} is dominant for the phase transition at T_Q. The plausible scenario is that the phase transition at T_Q is driven by the O_{xy}-type ferroquadrupolar ordering, as seen by the significant softening of C_{66}, positive g'_{xy}, and calculated results for O_{xy}.

[1] H. Sato, H. Sugawara, Y. Aoki, and H. Harima, in *Handbook of Magnetic Materials*, edited by K. H. J. Buschow (North-Holland, Amsterdam, 2009), Vol. 18, Chap. 1.

[2] Y. Kuramoto, H. Kusunose, and A. Kiss, J. Phys. Soc. Jpn. **78**, 072001 (2009).

[3] T. Onimaru and H. Kusunose, J. Phys. Soc. Jpn. **85**, 082002 (2016).

[4] I. Ishii, K. Takezawa, T. Mizuno, S. Kamikawa, H. Ninomiya, Y. Matsumoto, S. Ohara, K. Mitsumoto, and T. Suzuki, J. Phys. Soc. Jpn. **87**, 013602 (2018).

[5] I. Ishii, K. Takezawa, T. Mizuno, S. Kumano, T. Suzuki, H. Ninomiya, K. Mitsumoto, K. Umeo, S. Nakamura, and S. Ohara, Phys. Rev. B **99**, 075156 (2019).

[6] I. Ishii, T. Mizuno, S. Kumano, T. Umeno, D. Suzuki, Y. Kurata, T. Suzuki, D. I. Gorbunov, M. S. Henriques, and A. V. Andreev, Phys. Rev. B **101**, 165116 (2020).

[7] I. Ishii, T. Mizuno, K. Takezawa, S. Kumano, Y. Kawamoto, T. Suzuki, D. I. Gorbunov, M. S. Henriques, and A. V. Andreev, Phys. Rev. B **97**, 235130 (2018).

[8] D. I. Gorbunov, T. Nomura, I. Ishii, M. S. Henriques, A. V. Andreev, M. Doerr, T. Stöter, T. Suzuki, S. Zherlitsyn, and J. Wosnitza, Phys. Rev. B **97**, 184412 (2018).

[9] D. I. Gorbunov, I. Ishii, Y. Kurata, A. V. Andreev, T. Suzuki, S. Zherlitsyn, and J. Wosnitza, Phys. Rev. B **101**, 094415 (2020).

[10] I. Ishii, D. Suzuki, T. Umeno, Y. Kurata, Y. Wada, T. Suzuki, A. V. Andreev, D. I. Gorbunov, A. Miyata, S. Zherlitsyn, and J. Wosnitza, Phys. Rev. B **103**, 195151 (2021).

[11] P. Javorský, P. Burlet, E. Ressouche, V. Sechovský, H. Michor, and G. Lapertot, Phys. B: Condens. Matter **225**, 230 (1996).

[12] P. Javorský, H. Nakotte, R. A. Robinson, and T. M. Kelley, J. Magn. Magn. Mater. **186**, 373 (1998).

[13] B. J. Korte, V. K. Pecharsky, and K. A. Gschneidner, J. Appl. Phys. **84**, 5677 (1998).

[14] P. Javorský, M. Diviš, H. Sugawara, H. Sato, and H. Mutka, Phys. Rev. B **65**, 014404 (2001).

[15] P. Javorský, H. Mutka, and H. Nakotte, Appl. Phys. A **74**, S658 (2002).

[16] P. Javorský, P. Daniel, E. Šantavá, and J. Prchal, J. Magn. Magn. Mater. **316**, e400 (2007).

[17] Ł. Gondek, J. Czub, A. Szytuła, Z. Izaola, and E. Kemner, Solid State Commun. **149**, 1596 (2009).

[18] T. Suzuki, I. Ishii, N. Okuda, K. Katoh, T. Takabatake, T. Fujita, and A. Tamaki, Phys. Rev. B **62**, 49 (2000).

[19] Y. Nemoto, T. Yamaguchi, T. Horino, M. Akatsu, T. Yanagisawa, T. Goto, O. Suzuki, A. Dönni, and T. Komatsubara, Phys. Rev. B **68**, 184109 (2003).

[20] Y. Nakanishi, T. Sakon, M. Motokawa, M. Ozawa, T. Suzuki, and M. Yoshizawa, Phys. Rev. B **68**, 144427 (2003).

[21] T. Yanagisawa, T. Goto, Y. Nemoto, S. Miyata, R. Watanuki, and K. Suzuki, Phys. Rev. B **67**, 115129 (2003).

[22] T. Goto, Y. Nemoto, K. Sakai, T. Yamaguchi, M. Akatsu, T. Yanagisawa, H. Hazama, K. Onuki, H. Sugawara, and H. Sato, Phys. Rev. B **69**, 180511(R) (2004).

[23] M. Akatsu, T. Goto, O. Suzuki, Y. Nemoto, S. Nakamura, S. Kunii, and G. Kido, Phys. Rev. Lett. **93**, 156409 (2004).

[24] I. Ishii, H. Muneshige, Y. Suetomi, T. K. Fujita, T. Onimaru, K. T. Matsumoto, T. Takabatake, K. Araki, M. Akatsu, Y. Nemoto, T. Goto, and T. Suzuki, J. Phys. Soc. Jpn. **80**, 093601 (2011).

[25] I. Ishii, H. Muneshige, S. Kamikawa, T. K. Fujita, T. Onimaru, N. Nagasawa, T. Takabatake, T. Suzuki, G. Ano, M. Akatsu, Y. Nemoto, and T. Goto, Phys. Rev. B **87**, 205106 (2013).

[26] S. Kamikawa, I. Ishii, K. Takezawa, T. Mizuno, T. Sakami, F. Nakagawa, H. Tanida, M. Sera, T. Suzuki, K. Mitsumoto, and X. Xi, Phys. Rev. B **96**, 155131 (2017).

[27] D. I. Gorbunov, I. Ishii, T. Nomura, M. S. Henriques, A. V. Andreev, M. Uhlarz, T. Suzuki, S. Zherlitsyn, and J. Wosnitza, Phys. Rev. B **99**, 054413 (2019).

[28] A. V. Andreev, N. V. Mushnikov, T. Goto, and J. Prchal, Phys. B: Condens. Matter **346-347**, 201 (2004).

[29] T. J. Moran and B. Lüthi, Phys. Rev. **187**, 710 (1969).

[30] B. Wolf, B. Lüthi, S. Schmidt, H. Schwenk, M. Sieling, S. Zherlitsyn, and I. Kouroudis, Phys. B: Condens. Matter **294-295**, 612 (2001).

[31] M. T. Hutchings, Solid State Phys. **16**, 227 (1964).

[32] B. Lüthi, in *Dynamical Properties of Solids*, edited by G. K. Horton and A. A. Maradudin (North-Holland, Amsterdam, 1980), Chap. 4.

[33] See Supplemental Material of Ref. [5].

[34] Y. P. Varshni, Phys. Rev. B **2**, 3952 (1970).

[35] Z. Zhang, V. Keppens, and T. Egami, J. Appl. Phys. **102**, 123508 (2007).

[36] T. Suzuki, M. Nohara, Y. Maeno, T. Fujita, I. Tanaka, and H. Kojima, J. Supercond. **7**, 419 (1994).

[37] N. V. Hieu, T. Takeuchi, H. Shishido, C. Tonohiro, T. Yamada, H. Nakashima, K. Sugiyama, R. Settai, T. D. Matsuda, Y. Haga, M. Hagiwara, K. Kindo, S. Araki, Y. Nozue, and Y. Ōnuki, J. Phys. Soc. Jpn. **76**, 064702 (2007).

[38] S. Kamikawa, I. Ishii, Y. Noguchi, H. Goto, T. K. Fujita, F. Nakagawa, H. Tanida, M. Sera, and T. Suzuki, J. Phys. Soc. Jpn. **85**, 074604 (2016).

[39] M. Sera, H. Nohara, M. Nakamura, H. Tanida, T. Nishioka, and M. Matsumura, Phys. Rev. B **88**, 100404(R) (2013).

[40] R. Shiina, H. Shiba, and P. Thalmeier, J. Phys. Soc. Jpn. **66**, 1741 (1997).

[41] See, https://mgml.eu.